Adsorption Behavior and Wettability of Rhodochrosite Surface: Effect of C$_{18}$ Fatty Acid Unsaturation

Zhihui Shen [1], Qin Zhang [2,3,4,*], Xianbo Li [3,4] and Qianlin Chen [5]

[1] College of Resources and Environmental Engineering, Guizhou University, Guiyang 550025, China; zhshen@gzu.edu.cn

[2] Guizhou Academy of Science, Guiyang 550001, China

[3] National & Local Joint Laboratory of Engineering for Effective Utilization of Regional Mineral Resources from Karst Areas, Guiyang 550025, China; xbli3@gzu.edu.cn

[4] Guizhou Key Laboratory of Comprehensive Utilization of Non-metallic Mineral Resources, Guiyang 550025, China

[5] School of Chemistry and Chemical Engineering, Guizhou University, Guiyang 550025, China; qlchen@gzu.edu.cn

* Correspondence: zq6736@163.com

Abstract: Mineral surface wettability and its regulation by the adsorption of collectors have an important influence on the flotation performance. The adsorption behavior of C$_{18}$ fatty acid with different unsaturation and its effect on rhodochrosite wettability was investigated with surface tension, contact angle, and atomic force microscopy (AFM) measurements. The results indicated that rhodochrosite hydrophobicity increased with the increasing concentration of fatty acid, along with the maximum contact angle (θ_{max}) between hemimicelle concentration (HMC) and critical micelle concentration (CMC). Oleic acid (OA), linoleic acid (LA), and α-linolenic acid (ALA) had a higher θ_{max} than stearic acid (SA), but the value decreased with the increase of C=C bond number. Besides, preferential adsorption of unsaturated fatty acids on the liquid-air interface can be attributed to the molecule's steric hindrance resulting from C=C double bond, and the θ kept almost invariant with a higher value of Γ_{LG} than Γ_{SL} until HMC. The oriented monolayer and bilayer structure of fatty acids formed gradually on rhodochrosite surface with increasing concentration. However, the θ_{max} may not necessarily correspond to the beginning of bilayer formation. Cylindrical monolayer and bilayer micelles of SA molecules were observed on rhodochrosite surface at HMC and CMC, respectively. While bilayer structures of unsaturated fatty acids formed before complete coverage of monolayer on rhodochrosite surface because of surface heterogeneity. This work provided a good understanding on the adsorption mechanism of fatty acid on rhodochrosite for flotation.

Keywords: fatty acid; rhodochrosite; adsorption behavior; wettability; morphology

1. Introduction

Wettability plays a significant role in numerous industrial processes, such as flotation, oil recovery, coating, detergency, and cosmetics industry [1–3]. The wettability of a solid surface could be significantly affected by the adsorption of surfactants owing to the change of interface properties in solid-liquid-air systems, resulting in the extensive use in mineral flotation [4,5]. The mineral surface property, especially the wettability, is the key to flotation. The flotation efficiency mostly depends on using surfactants, especially the collector. Therefore, minerals surface wettability and its regulation by the adsorption of the collector are the core issues in the flotation process [6,7].

Rhodochrosite is the foremost valuable mineral in manganese resources. However, low-grade manganese ore accounts for over 90% of manganese resources in China, which need to be beneficiated [8]. Flotation is regarded as a widely used and effective method for rhodochrosite beneficiation, showing various advantages over other conventional techniques [9–11]. There are many kinds of rhodochrosite flotation collectors, including anionic collector [12–14], cationic collector [15,16] and nonpolar collector [17]. Among these collectors, the fatty acid has been commonly used due to its low cost and extensive source [18]. The hydrocarbon chain lengths, unsaturation degree, carbon-chain isomerism, and frothing property of fatty acid could influence its collection performance. The solubility, cross-sectional area, and molecular curvature of fatty acid increase with the increase of unsaturation, which significantly affects the effective concentration of fatty acid in aqueous solution and its adsorption activity and capacity on the mineral surface [19]. Therefore, it is significant to explore the adsorption behavior of unsaturated fatty acid and its effect on the wetting behavior of rhodochrosite.

Over the years, many studies about the adsorption mechanism of fatty acid on calcite, fluorite, apatite, and other minerals in flotation have been carried out by researchers, with atomic force microscopy (AFM), infrared spectroscopy, and first-principles calculations methods [20–24]. Ye [20] indicated that the hydrophobicity of collophane can be enhanced by concomitant monolayer and bilayer micelles of oleate above HMC, and effect of adsorbed structure on wettability of collophane was confirmed by MDS. Xie [21] investigated adsorption of fatty acid on fluorapatite (001) surface based on DFT. The results showed that as the carbon chain grew within certain limits, the adsorption became stronger, and fatty acid formed stable chemical adsorption and hydrogen bond adsorption configurations at Ca1 (surf) site of Ca termination. Young [23] suggested that chemisorption of oleate on calcite surface occurs at low oleate concentrations, and the adsorption densities decrease with increasing temperature based on the in-situ FT-NIR/IRS. Moreover, the effect of fatty acid unsaturation degree on mineral hydrophobicity and flotation performances have been investigated. Iwasaki [25] and Purcell [26] et al. suggested that higher recoveries of rutile or hematite can be obtained with higher adsorption acted by oleic acid (OA) than that by linoleic acid (LA) and α-linolenic acid (ALA) at pH greater than 8. It was found that fatty acid with a higher unsaturation degree has less surface activity because of higher solubility. Liu et al. [27] investigated that the effect of iodine value of sodium fatty acids on collophane flotation, which suggested that stronger hydrophobicity of collophane attributes to a higher iodine value, and flotation recovery positively correlates with iodine value. In addition, Wang et al. [28] calculated that the frontier molecular orbital energies difference of LA was lower than that of OA, resulting in lower chemical activity and adsorption stability of OA on diaspore.

However, the mechanism research on fatty acid and rhodochrosite mainly focuses on the effect of structural modification on collecting capacity and solution chemistry for fatty acid. Zhou et al. [29,30] suggested that linoleate hydroxamic acid (LHA) showed superior selectivity in the flotation of rhodochrosite, along with the chemisorption of a five-membered chelate ring of LHA on rhodochrosite surface. The adsorption of LHA onto rhodochrosite leads to the formation of hydrophobic agglomerates of rhodochrosite particles (Mn-LHA compounds or chelates) which enhance the floatability of rhodochrosite. Chen et al. [31] concluded that surface activity and collecting capability of the fatty acid amide collectors increased with the increasing C=C double bond numbers in the long chain. Dai et al. [32] also suggested that hydroxamic acid collectors were adsorbed on the rhodochrosite surface physically and chemically. Besides, the formation of manganese oleate precipitation and non-electrostatic forces between rhodochrosite and sodium oleate were the keys for flotation, which was explained by Qin et al. [33]. Bu et al. [34] indicated that rhodochrosite interacted with oleic acid and sodium dodecyl benzene sulfonate, resulting in a more negative zeta potential and the co-adsorption of the collector and synergist. Moreover, chemical adsorption of the hydroxamic acid on rhodochrosite led to negative shifts for the zeta potential of rhodochrosite, which concluded by Zhao et al. [35]. In summary, research on the adsorption effect of fatty acid on rhodochrosite is limited, especially the effect of the unsaturation degree of fatty acid on the wettability of rhodochrosite. Four fatty acids containing 18 carbon atoms and a different number of C=C double bonds (0~3) were used in this

work. By surface tension measurements, contact angle measurements, and AFM measurements, the adsorption properties of fatty acid at solution-air and rhodochrosite-solution interfaces with rhodochrosite wettability have been investigated, which provides a good understanding of the adsorption mechanism of fatty acids on rhodochrosite for flotation applications.

2. Materials and Methods

2.1. Materials

Natural rhodochrosite was obtained from Guangxi province, China. The mineral composition was measured by X-ray diffraction analysis (XRD) (X'Pert PRO, Panalytical Company, Almelo, The Netherlands) (see Figure 1), and the diffraction peak of natural rhodochrosite shows a good agreement with the standard card (PDF#44-1472). The rhodochrosite was cut into a lump of nearly 1 cm in length, width, and thickness, respectively. Then the lump was polished using grit silicon carbide papers of 500, 1000, and 2000 mesh, and polished using a grinding machine (YMP-2B, from Shanghai Metallurgical Equipment Company Ltd., Shanghai, China). Grit silicon carbide papers of 500, 1000, and 2000 mesh were used as the abrasive materials, silk cloth and alumina powders of 1.0, 0.3, and 0.05 mm were used as the polishing materials, both were obtained from Lab Testing Technology (Shanghai) Co., Ltd., Shanghai, China [20]. The ultrasonication with water, ethanol, and ultrapure water was used to wash the lump successively for the contact angle and the AFM measurements.
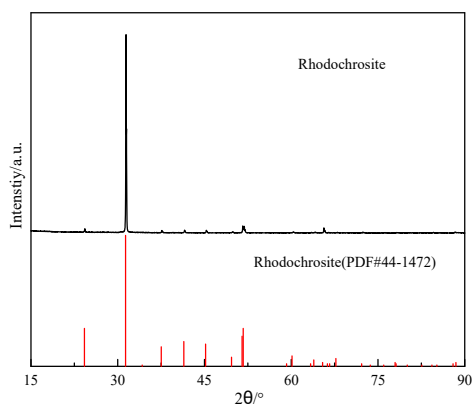

Figure 1. XRD pattern of the rhodochrosite and corresponding PDF standard card.

The C_{18} fatty acids including stearic acid (SA), OA and LA used in this work were analytically pure and purchased from Shanghai Aladdin Bio-Chem Technology Co. Ltd. (Shanghai, China). In contrast, ALA was 85% pure and purchased from Shanghai Jizhi Bio-Chem Technology Co. Ltd. (Shanghai, China). The molecular structure and mainly physical properties of the above fatty acids are shown in Figure 2 and Table 1, respectively. Deionized water with the resistivity of 18.25 MΩ·cm was used to prepare the solutions of known concentration.

Table 1. Mainly physical properties of C_{18} fatty acid.

C_{18} Fatty Acid	Structure and Degree of Saturation	Theoretically Calculated Length/nm	Limiting Area of Monolayer (Å²)	Intermolecular Distance in Monolayer (Å)	Melting Temperature (°C) [a]
SA	18:0	2.62–2.66 [36]	20 [36,37]	4.47 [38]	69–71
OA	18:1; (cis)9	2.48–2.52 [36]	41 [36,39]	6.40 [38]	13–14
LA	18:2; (cis)9,12	2.40–2.44 [36]	48 [36,40]	6.93 [38]	−5~−1
ALA	18:3; (cis)9,12,15	_[b]	_[b]	_[b]	−11~−10

[a] Sigma-Aldrich catalog. [b] It is difficult to obtain the values of length and limiting area for ALA due to its inherent molecule characteristics.
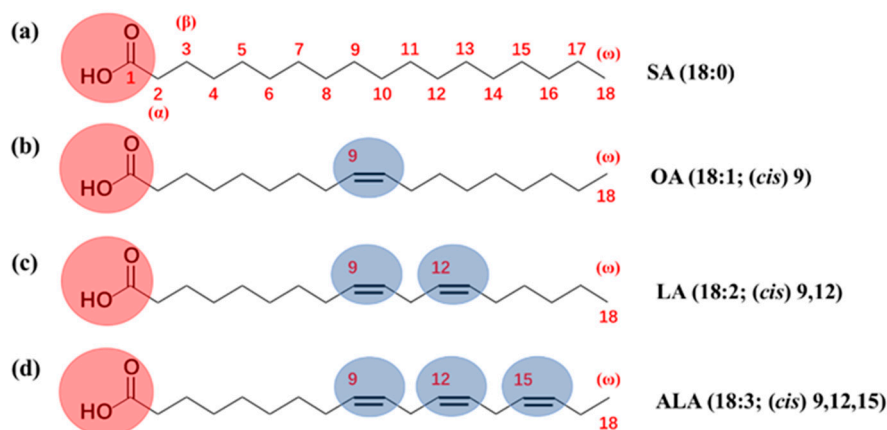
Figure 2. Molecular structures and saturation degree of SA, OA, LA and ALA.

2.2. Methods

2.2.1. Measurements of Surface Tension

The Wilhelmy plate method with a surface tensiometer (JK99B, Powereach, Shanghai, China) under atmospheric pressure was used for surface tension measurement of fatty acid aqueous solutions. The glassware and platinum plate were cleaned and washed by ethyl alcohol and deionized water in sequence, and the platinum plate was treated with alcohol flame to remove any organic contamination. Before sample measurement, the surface tension of deionized water at 25 °C was tested to examine the cleanliness of glassware and plate and correct the tensiometer. Approximately 25 mL fatty acid solution was used for each test. Each sample was tested at least three times in succession.

2.2.2. Measurements of Contact Angle

The dynamic contact angle measuring instrument (HARKE-SPCAX3, Beijing Hake test instrument factory, Beijing, China) was used for contact angle (θ) measurements for fatty acid solutions on rhodochrosite with the sessile drop method. The rhodochrosite lump was immersed in a 50 mL fatty acid solution for 20 min. Next, the sample was taken out and dried at atmospheric temperature. The droplet volume used for contact angle test is 2 microliters. In order to avoid the gravity influence of the droplet, the θ was measured 10 s after the droplet falls on the rhodochrosite surface. The "baseline circle" in the instrument's software was used. Each θ was measured three times at different surface areas, and the average value was the final result [41]. After each test, the rhodochrosite lump was successively washed with ethyl alcohol and deionized water. Finally, the lump was heated at 40 °C for 30 min for the next test.

2.2.3. AFM Analysis

The adsorption morphology and thickness of fatty acid on rhodochrosite surface was visualized by the AFM, a Dimension Icon (Bruker, Karlsruhe, Germany). The ScanAsyst-Air tips (Bruker, Karlsruhe, Germany) with peak force tapping mode at 1 Hz scan rate and 512 lines per sample was used for collecting the images. First, the surface of polished rhodochrosite was visualized to record an AFM image for comparison. Then the rhodochrosite lump was immersed in a 50 mL fatty acid solution for 20 min. Next, the sample was taken out and dried at atmospheric temperature. Finally, AFM images of the surface adsorbed fatty acid were recorded. The AFM images were analyzed by Nanoscope Analysis 1.40 software (Bruker, Karlsruhe, Germany) with a first order smoothing firstly, and then the roughness module was used to analyze the entire image roughness. Finally, the corresponding height profiles were obtained with the Section module [42].

3. Results and Discussion

3.1. Self-Assembly of Fatty Acid in Aqueous Solution

The self-assembly of fatty acids can form micelles in aqueous solutions, depending on their critical micelle concentration (CMC) [43]. The relationship between equilibrium surface tension (γ_{LG}) and concentration of four fatty acids are presented in Figure 3. As shown in Figure 3, with the increase in the fatty acid concentration of the solutions, the γ_{LG} of all fatty acids decrease until they are stable. The values of the premicellar concentration [44], the CMC, and surface tension at the CMC (γ_{CMC}) of fatty acid can also be obtained from Figure 3, as shown in Table 2. The premicellar concentration and CMC of OA, LA, and ALA are 1×10^{-5} mol/L and 1×10^{-3} mol/L, respectively, which are consistent with other researches [41,45]. The premicellar concentration and CMC of SA are 1×10^{-6} mol/L and 1×10^{-4} mol/L, respectively, which are lower than those of OA, LA, and ALA. SA is a saturated fatty acid, and its melting point is higher than unsaturated acids with C=C double bond, resulting in stronger hydrophobicity and lower value of CMC of SA. For unsaturated fatty acids, OA has the smallest value of γ_{CMC}, while ALA has the largest γ_{CMC}, which may be due to that the greater number of C=C bond in ALA, the less hydrophobic of the carbon chain, resulting in higher γ_{LG} when micelles are formed, indicating that the unsaturation degree also affects the self-assembly of fatty acids. This conclusion is supported by other literature [46]. It is considered that small micelles may be formed in the range of fatty acid concentrations ranging from the premicellar concentration to CMC, while spherical micelles may be formed at the CMC. Schematic plots of the correspondent micelles are shown in Figure 4.
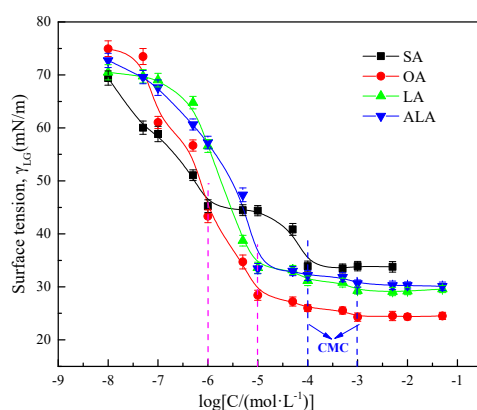

Figure 3. Surface tension variation as a function of the fatty acid concentration.

Table 2. The premicellar concentration, CMC and γ_{CMC} of studied fatty acid at 25 °C.

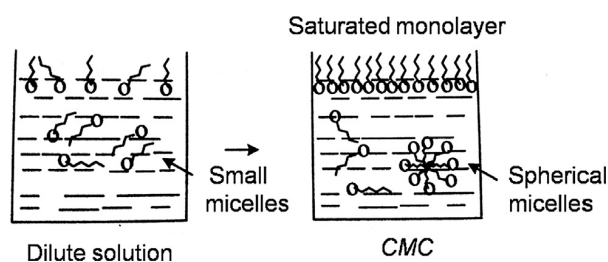| Fatty Acid	Premicellar Concentration (mol/L)	CMC (mol/L)	γ_{CMC} (mN/m)
SA	1×10^{-6}	1×10^{-4}	33.915
OA	1×10^{-5}	1×10^{-3}	24.298
LA	1×10^{-5}	1×10^{-3}	29.298
ALA	1×10^{-5}	1×10^{-3}	30.631

Figure 4. Micellization of the surfactant solution [43].

3.2. Wettability of Rhodochrosite

The dependence of θ of rhodochrosite on the total concentration of four fatty acids in aqueous solutions is shown in Figure 5. As shown in Figure 5, the θ keeps almost constant over the low range of fatty acid concentration. While the θ and surface hydrophobicity of rhodochrosite increases with the increasing fatty acid concentration. When the concentration of SA is 5×10^{-6} mol/L, and the concentration of OA, LA and ALA are 5×10^{-5} mol/L, the maximum contact angle (θ_{max}) is 67.50°, 76.20°, 75.87°, and 72.60°, respectively. It suggests that the rhodochrosite may be the most hydrophobic between hemimicelle concentration (HMC) and CMC for fatty acids. However, there is a more marked decrease in θ for all fatty acids with a further increase in concentrations. When it exceeds CMC, the θ decreases rapidly, and rhodochrosite becomes hydrophilic with the rise in concentration, indicating that the mineral surface becomes hydrophilic again with increasing fatty acid concentration.
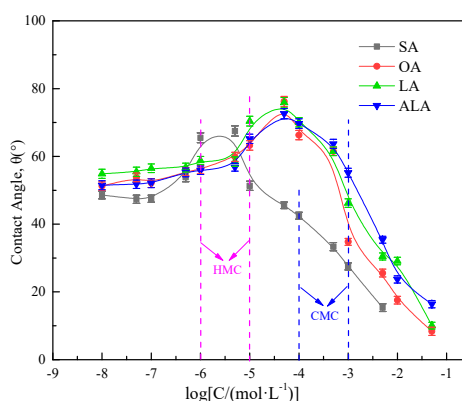

Figure 5. Variation of θ with fatty acids concentration.

The θ_{max} for three unsaturated acids are significantly larger than that for SA. The reason may be that the greater the unsaturation degree, the lower the melting point (Table 1), and the easier it is to dissolve and disperse in water. Figure 5 also shows that for OA, LA, and ALA, the θ_{max} decrease with increase in C=C bond number of fatty acids, the reason may be that the more C=C double bond, the larger the unsaturation degree, the molecular distance and limit area of unsaturated fatty acid (data in Table 1: OA < LA < ALA). Therefore, the adsorption of unsaturated fatty acid on the surface of rhodochrosite is more affected by the steric hindrance caused by its curved structure [47]. Moreover, there is also an increase in chain disorder within the adsorbed layer as the unsaturation increases, hence increased effective surface space required, resulting in lower packing density of unsaturated alkyl chains. This is also supported by Wood et al. [48]. At the same concentration, the number of fatty acid molecules adsorbed on the rhodochrosite surface are OA > LA > ALA, and the adsorption density of fatty acid on rhodochrosite is proportional to its molecule number, resulting in the weaker hydrophobicity of rhodochrosite with an increase in C=C bond number of fatty acids.

3.3. Adsorption at Rhodochrosite-Water and Air-Water Interface

3.3.1. Dependence of Wettability and Surface Tension

According to literature, the critical surface tension of wetting can be estimated by extrapolation of cosθ versus surface tension γ_{LG} plots to cosθ = 1 [49,50]. As shown in Figure 6, it appears that there is no linear correlation between cosθ and γ_{LG}. However, the cosθ is correlated with γ_{LG} within a certain range of γ_{LG}.
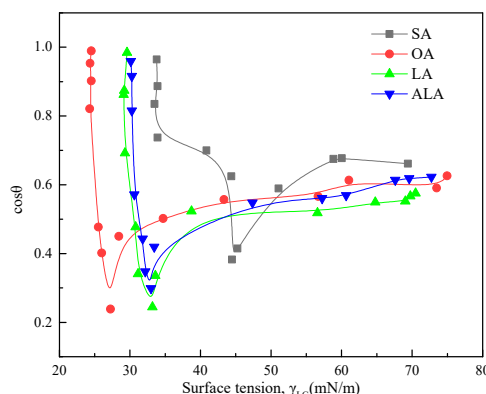
Figure 6. The variation of cosθ with γ_{LG} of fatty acid solutions.

The value of cosθ gradually decreases with the decrease in γ_{LG} of four fatty acid solutions, resulting in the increase of hydrophobicity for rhodochrosite. However, the change rate of rhodochrosite hydrophobicity versus γ_{LG} is lower. During the adsorption of SA, OA, LA, and ALA, the minimum values of cosθ are 0.38, 0.24, 0.24 and 0.30, respectively, with the highest hydrophobicity of rhodochrosite. At this time, the corresponding γ_{LG} of SA, OA, LA, and ALA are 44.47, 27.23, 33.19 and 32.98 mN/m, respectively. However, the slope of cosθ-γ_{LG} curves quickly increase with a marked increase in cosθ which eventually approaching 1 with a further decrease in γ_{LG}, indicating that as the bulk concentration continues to rise, the surface of rhodochrosite changes from hydrophobic to hydrophilic, and finally strongly hydrophilic. At this time, the γ_{LG} of SA, OA, LA, and ALA correspond to the minimum values of 33, 24, 29 and 30, respectively.

3.3.2. Relationship between the Adhesion and Surface Tension

According to literature, the relationship between adhesion tension ($\gamma_{LG}\cdot$cosθ) and γ_{LG} for both hydrophilic and hydrophobic solids is possible to be established [51–53], as shown in Equation (1):

$$\gamma_{LG}\cos\theta = a\gamma_{LG} + b \tag{1}$$

where a and b are constants, depending on the solid surface property. Besides, Combining the Young's equation and Gibbs equation, Lucassen-Reynders proposed a simple method to analyze the relationship between adsorption and equilibrium wetting, as shown in Equation (2) [54]:

$$\frac{d(\gamma_{LG}\cos\theta)}{d\gamma_{LG}} = \frac{\Gamma_{SG} - \Gamma_{SL}}{\Gamma_{LG}} \tag{2}$$

where Γ_{SG}, Γ_{SL} and Γ_{LG} represent the excess surface concentrations of surfactants at the solid-air, solid-liquid, and liquid-air interfaces, respectively. Assuming that $\Gamma_{SG} \approx 0$, it is possible to obtain the Γ_{SL}/Γ_{LG} value via calculating the slope of the $\gamma_{LG}\cdot$cosθ-γ_{LG} curve. Therefore, combining Equations (1) and (2), Equation (3) can be obtained.

$$\frac{\Gamma_{SL}}{\Gamma_{LG}} = -a \tag{3}$$

From Equations (1) and (2), the critical surface tension of solid wetting would be determined, and surfactant adsorption on the liquid-air and solid-liquid interfaces would be analyzed. As weak interaction (such as Lifshitz-van der Waals interactions) presented in the surfactant and solid, the slope of the $\gamma_{LG}\cdot$cosθ-γ_{LG} curve is less than 1, while the slope is greater than 1 as strong interaction presented (such as electrostatic interaction) [55,56].

The variation of $\gamma_{LG}\cdot$cosθ with γ_{LG} of fatty acid solutions was presented in Figure 7. As shown in Figure 7, there is no direct linear trend between $\gamma_{LG}\cdot$cosθ and γ_{LG} on the rhodochrosite-fatty acid solutions-air interface. However, within a certain concentration range, the $\gamma_{LG}\cdot$cosθ changes linearly

with the γ_{LG}. For SA, with reduction in γ_{LG}, the value of *a* varies from 0.57 to 1.97, the $\gamma_{LG}\cdot\cos\theta$ decreases and suddenly increases around γ_{CMC}. In the initial adsorption period, the ratio of Γ_{SL} to Γ_{LG} (a) is less than 1, that is, $\Gamma_{SL} < \Gamma_{LG}$, indicating that the adsorption density on the solid-liquid interface is lower than that on the air-liquid interface. As γ_{LG} continues to decrease, the *a* value increases to 1.24 (~1), which shows that the Lifshitz-van der Waals interactions between fatty acid molecules and rhodochrosite is the primary force of adsorption. While the electrostatic force interaction mainly drives the adsorption, $\Gamma_{SL} > \Gamma_{LG}$ and the slope value >1 [55]. In the case of OA, LA, and ALA, the variations of $\gamma_{LG}\cdot\cos\theta$ and γ_{LG} are similar. The $\gamma_{LG}\cdot\cos\theta$ decrease with the decreasing γ_{LG} and then increase rapidly at γ_{CMC} with no stable region in the $\gamma_{LG}\cdot\cos\theta$-$\gamma_{LG}$ curves. From the values of the slope, Van der Waals force is the primary interaction in the initial adsorption process. However, the steric hindrance effect and chain disorder produced by the molecular structure with C=C double bond makes it more difficult for unsaturated fatty acids to adsorb on rhodochrosite [47], resulting in the ratio of Γ_{SL} to Γ_{LG} slightly smaller than 1. While the electrostatic interaction comes into operation, Γ_{SL} is much larger than Γ_{LG}, which causes a marked increase in the value of *a*.
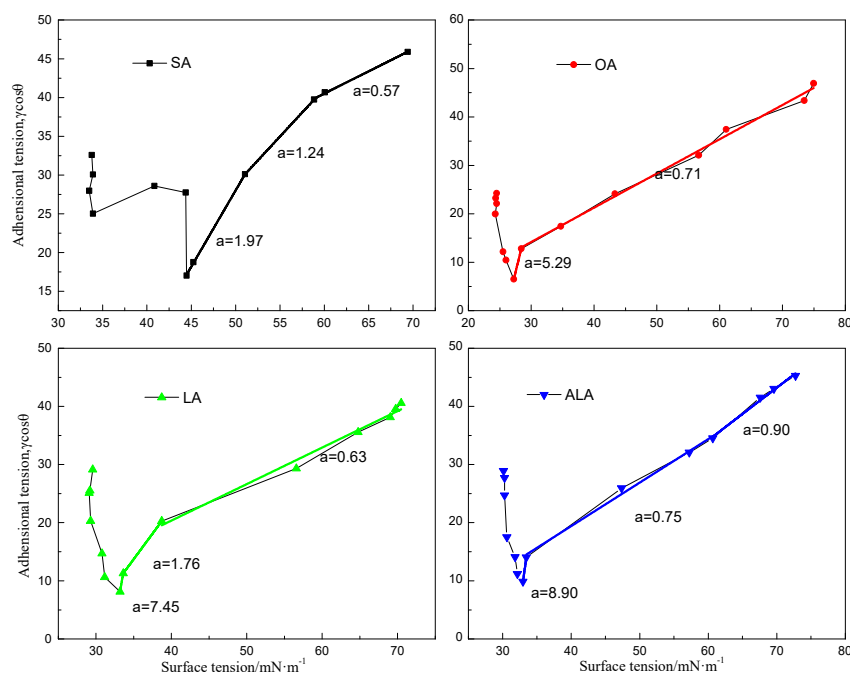

Figure 7. $\gamma_{LG}\cdot\cos\theta$ as a function of γ_{LG} of fatty acid solutions.

3.3.3. Work of Adhesion

Because the solid-liquid interfacial tension can be expressed by the following equation [57]:

$$\gamma_{SL} = \gamma_{LG} + \gamma_{SG} - W_A \tag{4}$$

where W_A is the adhesion work of the liquid to the solid surface. According to Young's equation, the θ depends on the solid-liquid interfacial tension(γ_{SL}), solid-air interfacial tension (γ_{SG}), and liquid-air interfacial tension (γ_{LG}), as shown in Equation (5):

$$\gamma_{SG} - \gamma_{SL} = \gamma_{LG}\cos\theta \tag{5}$$

Equation (6) can be obtained by introducing Equation (4) into Young's Equation (5):

$$W_A = \gamma_{LG}(\cos\theta + 1) \tag{6}$$

The W_A of fatty acid solutions to the rhodochrosite surface was calculated, as shown in Figure 8. It is suggested that the W_A for the aqueous solution of all fatty acids decreases first and then with increasing concentration. Interestingly, the minima values of the W_A of all fatty acids are also observed at the concentration around the HMC.
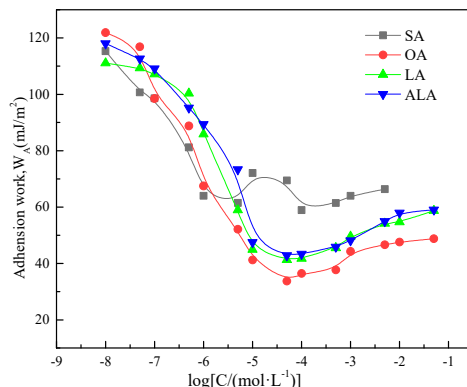

Figure 8. Variation of W_A with fatty acid concentration.

3.4. Structural Dependence of Fatty Acid on the Wettability of Rhodochrosite Surface

The dependencies of γ_{LG}, θ, $\gamma_{LG} \cdot \cos\theta$, and W_A on concentration and the results have been replotted in Figure 9 for four fatty acids. The variations in adhesional data as a function of increasing concentration can be divided into four stages. The probable diagrammatic drawing of the adsorbed fatty acid on the air-liquid interface and rhodochrosite-liquid interface in the four stages is presented in Figure 10.
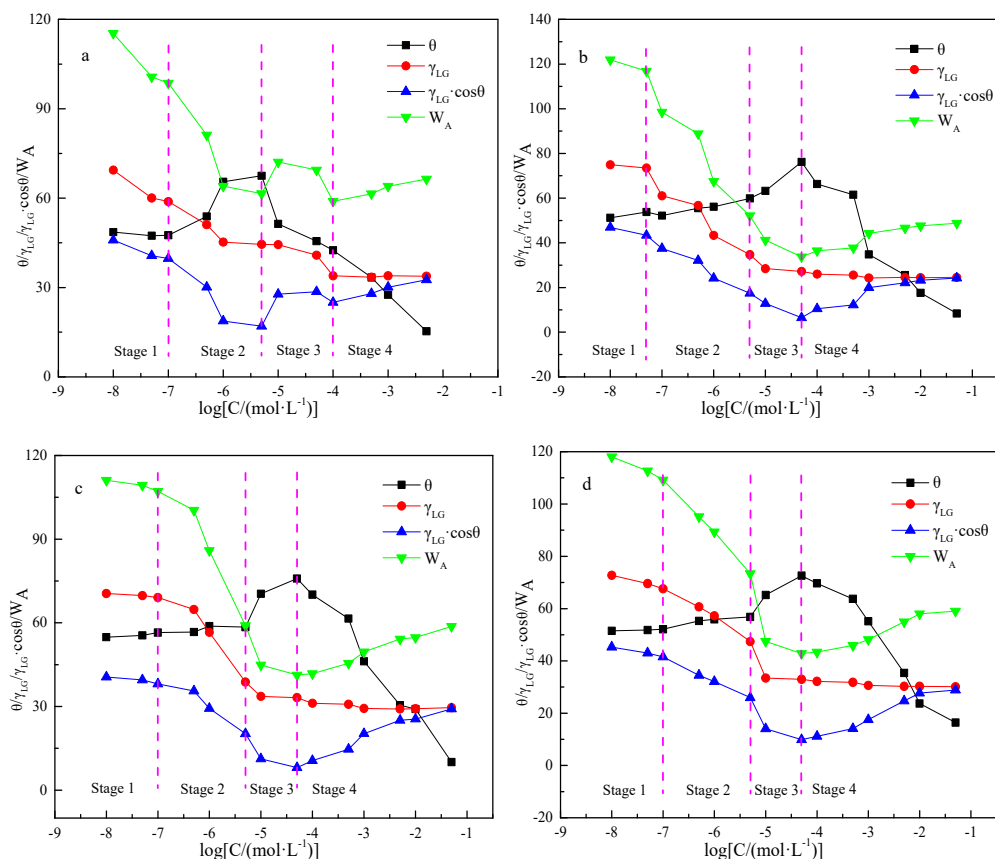

Figure 9. Adhesional data as a function of log C of fatty acid solutions (**a**: SA; **b**: OA; **c**: LA; **d**: ALA).
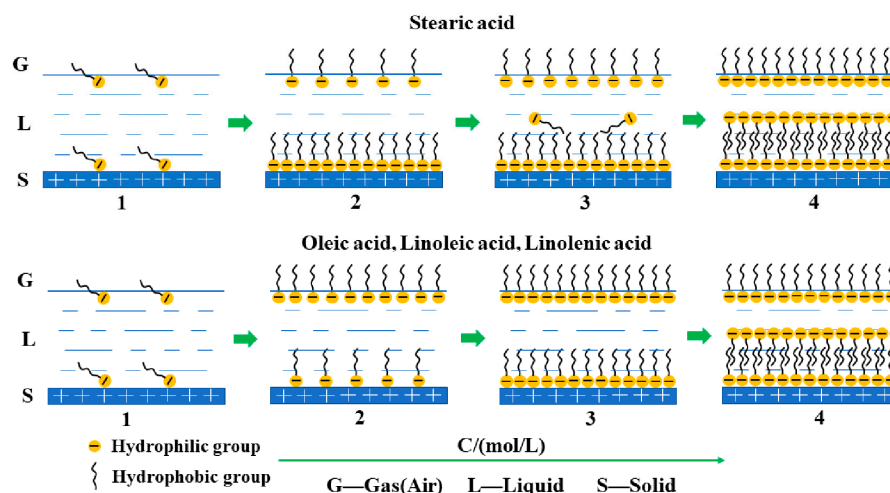
Figure 10. Adsorption schematic model of fatty acid on the rhodochrosite surface.

In the case of SA, as shown in Figure 9a, in stage 1, stable adsorption films are difficult to form on both liquid-air and rhodochrosite-liquid interfaces because of very low concentration. Therefore, the γ_{LG}, θ, $\gamma_{LG} \cdot \cos\theta$, and W_A all change little until 1×10^{-7} mol/L. In stage 2, the γ_{LG}, $\gamma_{LG} \cdot \cos\theta$, and W_A gradually decrease with increasing concentration, while the θ become larger and larger. The stable unsaturated adsorption film begins to form with SA molecules, resulting in enhanced hydrophobicity of rhodochrosite. At the early step of stage 2, under the action of Lifshitz-van der Waals forces, SA molecules adsorb with the hydrophilic group pointing to the rhodochrosite and the hydrophobic group to the solution. On the basis of results in Figure 7, $\Gamma_{SL} \approx \Gamma_{LG}$, leading to a slow increase in θ. Then, the anionic head group of SA begins to interact with the rhodochrosite surface via electrostatic forces, molecules preferentially adsorb at rhodochrosite-liquid interface and $\Gamma_{SL} \approx 2\Gamma_{LG}$. As a result, the θ increases sharply attributed to the relatively greater extent of decrease in $\gamma_{LG} \cdot \cos\theta$ than γ_{LG}. Besides, there are the θ_{max} and minimal $\gamma_{LG} \cdot \cos\theta$ as the concentration increasing to 5×10^{-5} mol/L, around the HMC, suggesting that a saturated monolayer adsorption film has formed at the rhodochrosite-liquid interface. In stage 3, SA molecules kept adsorbing at the liquid-air interface, the γ_{LG} decreases monofonically, and the θ decreases significantly. Then, the micelles will form with the addition of SA molecules and adsorb onto monolayer film at the rhodochrosite surface again through carbon-chain association, which leads to enhanced hydrophilicity of rhodochrosite. In stage 4, as the SA concentration reaches 1×10^{-4} mol/L (CMC), the γ_{LG} decreases to a minimum and remains stable, a saturated adsorption film forms with SA molecules at the liquid-air interface. However, the θ continues to decrease, and $\gamma_{LG} \cdot \cos\theta$ and W_A increase with a further increase in concentration. Hence the rhodochrosite is more hydrophilic attributed to the formation of the bilayer structure at a solid-liquid interface.

The variation of γ_{LG}, θ, $\gamma_{LG} \cdot \cos\theta$, and W_A with concentration for OA, LA, and ALA are similar. As shown in Figure 9b–d, in stage 2, the θ increases slowly with the decreases in γ_{LG} and $\gamma_{LG} \cdot \cos\theta$ for OA, while the θ keeps constant with the reductions in γ_{LG} and $\gamma_{LG} \cdot \cos\theta$ for LA and ALA. The reason may be that the unsaturated acid molecules mainly adsorb on the solid-liquid interface by van der Waals force with lower concentration. Meanwhile, in contrast to SA, the presence of C=C double bond makes unsaturated acids molecules more polar, reactive, and bent [58], which may increase the non-linear tendency of molecules, and reduce the adsorption space and amount of unsaturated fatty acid molecules on the surface of rhodochrosite [59]. On the other hand, the values of Γ_{SL} are smaller than Γ_{LG} in stage 2 for OA, LA, and ALA from the results in Figure 7, suggesting the dominant adsorption of acids on liquid-air interface. On the basis of Young's equation (Equation (5)), when $\theta < 90°$, the reduction of γ_{LG} will result in the decrease of θ, while the decline in the $\gamma_{LG} \cdot \cos\theta$ will lead to the increase of θ. Therefore, the θ remains almost stable at stage 2 attributed to the competition between γ_{LG} and $\gamma_{LG} \cdot \cos\theta$ [4]. In stage 3, the adsorption density of OA, LA, and ALA

in the rhodochrosite-liquid interface is higher than that in the air-liquid interface (OA: $\Gamma_{SL} \approx 5\Gamma_{LG}$, LA: $\Gamma_{SL} \approx 7\Gamma_{LG}$, ALA: $\Gamma_{SL} \approx 9\Gamma_{LG}$). At this time, the driving force for adsorption should be a stronger interaction (electrostatic attraction), which leads to an increase in γ_{SL}, a significant increase in the θ with enhanced hydrophobicity of rhodochrosite. When the concentration arriving at 5×10^{-5} mol/L, a saturated film forms at the liquid-air and rhodochrosite-liquid interface, resulting in the θ_{max} and strongest hydrophobicity of rhodochrosite. Therefore, as the concentration increases, the excessive acid molecules will be adsorbed on the saturated film, immediately forming a double-layer structure at the rhodochrosite-liquid interface (stage 4).

3.5. Morphology of Adsorbed Fatty Acid on Rhodochrosite Surface

In most research, mica is often used as a substrate because of its flatness [60]. Therefore, to accurately determine the fatty acid adsorption layer height, a very smooth rhodochrosite surface is required. A ground and polished rhodochrosite surface was used for the substrate in our research. The micrograph (Figure 11a) indicates that the surface of rhodochrosite is relatively flat, showing a certain streak, and accompanied by tiny voids. The surface roughness (Ra) of 5.77 nm can be obtained from the two-dimensional AFM image (Figure 11b).
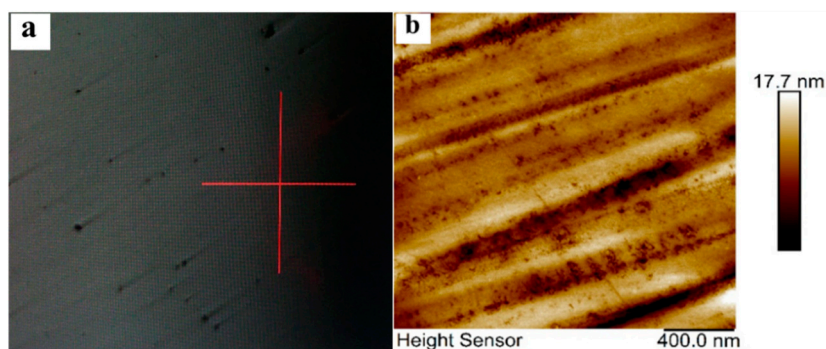

Figure 11. Micrographs of AFM images of a polished rhodochrosite surface. (**a**) Micrograph image, (**b**) two-dimensional AFM image.

The 2D AFM images of the rhodochrosite surface treated by four fatty acids solutions with two different initial concentrations are shown in Figure 12. The homologous height of adsorbed fatty acid on the rhodochrosite surface is shown in Figure 13. The two concentrations used are Premicellar concentration and CMC mentioned above in Table 2. Comparing Figure 12 with Figure 11, it is suggested that spotted, spherical, laminated, and block adsorption structures are evident on the surface of rhodochrosite after treated with fatty acid. From the height distribution diagram, the small and large columned micelles morphologies of adsorbed fatty acid were observed, and their heights were obtained. Moreover, by comparing the measured heights of the adsorption layer with the theoretical molecular length of the fatty acid, estimation for monolayer, bilayer, or multilayer structures of adsorbed fatty acid were carried out [20].
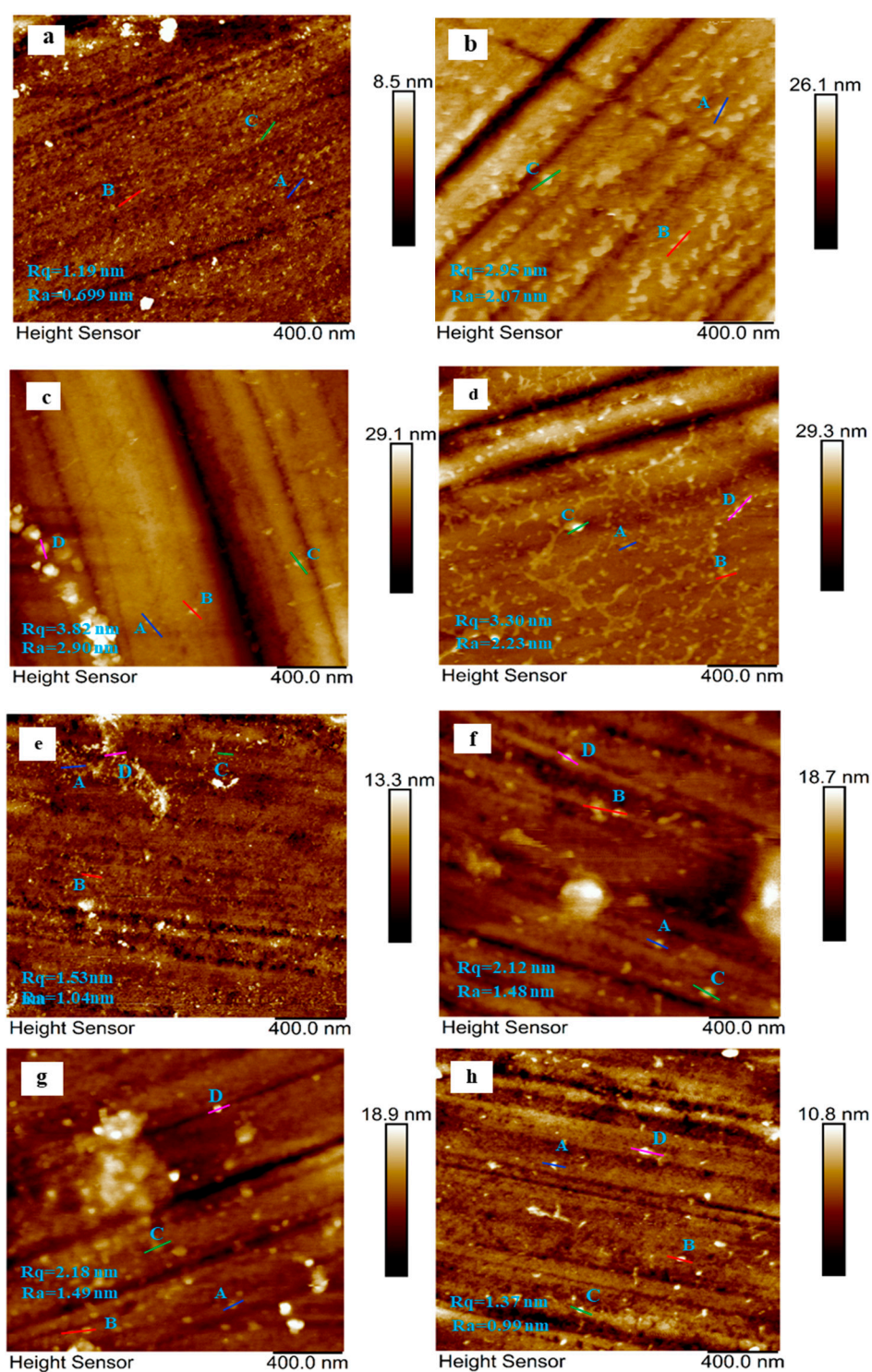
Figure 12. Two-dimensional AFM images of adsorbed fatty acid on rhodochrosite. (**a**) 1×10^{-6} mol/L SA, (**b**) 1×10^{-4} mol/L SA; (**c,e,g**) 1×10^{-5} mol/L OA, LA, ALA respectively; (**d,f,h**) 1×10^{-3} mol/L OA, LA, ALA respectively. The blue, red, green and carmine lines represent the transverse section position of adsorbed fatty acid.
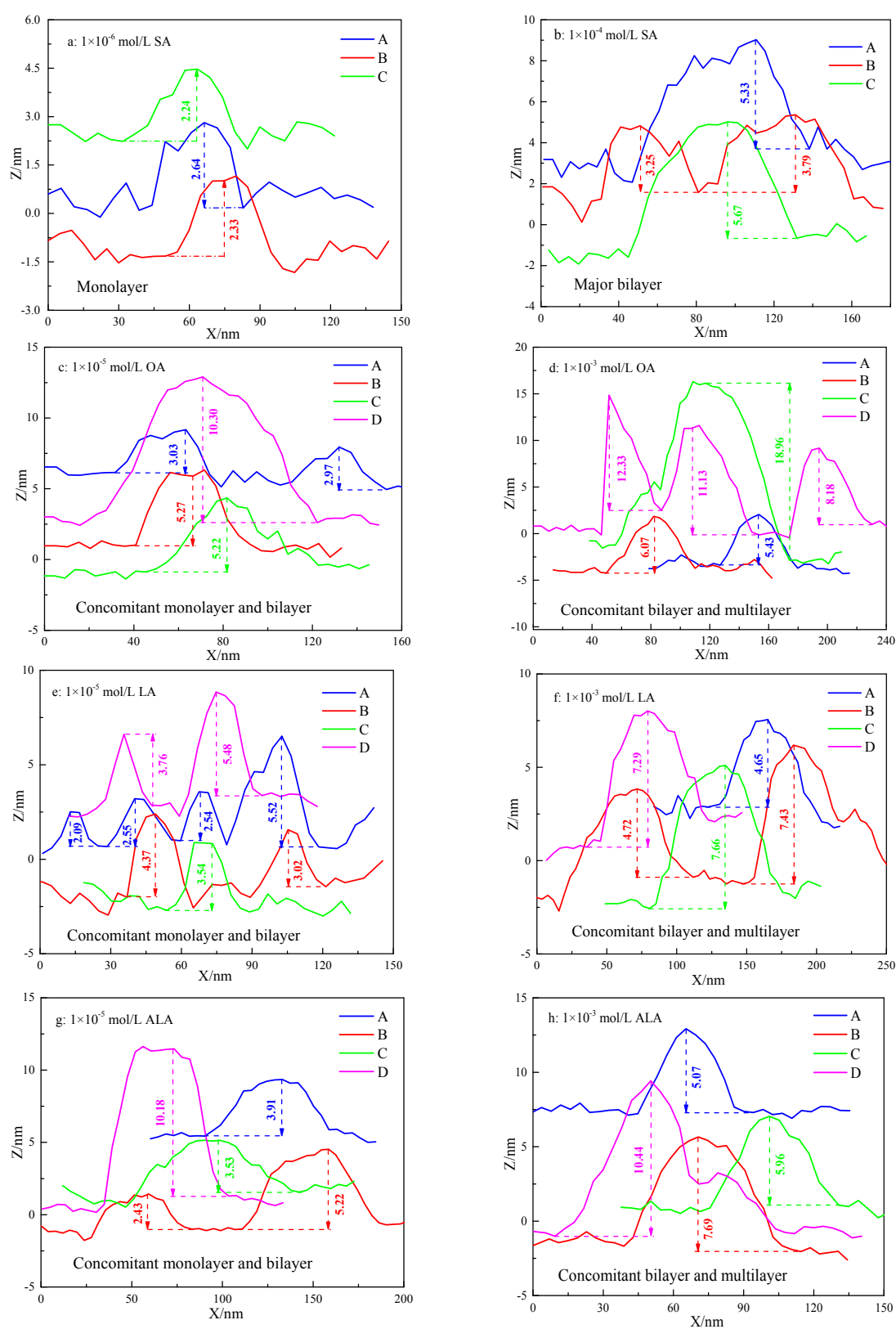
Figure 13. The homologous height of adsorbed fatty acids in the transverse section position of Figure 12, (**a**) 1×10^{-6} mol/L SA, (**b**) 1×10^{-4} mol/L SA; (**c,e,g**) 1×10^{-5} mol/L OA, LA, ALA respectively; (**d,f,h**) 1×10^{-3} mol/L OA, LA, ALA respectively.

In the case of SA, the theoretically calculated molecular length range from 2.62 to 2.66 nm (Table 1). When the concentrations were 1×10^{-6} mol/L and 1×10^{-4} mol/L, the adsorption layer heights were in the range of 2.24–2.64 nm and 3.25–5.67 nm, respectively. This indicates that the small cylindrical micelles with monolayer formed at HMC, while large columned micelles with monolayer and bilayer formed at CMC (Figure 12a,b, Figure 13a,b). For OA, LA, and ALA, the adsorption layer heights were in the range of 2.97–10.30 nm, 2.09–5.52 nm, 2.43–10.18 nm at the concentration of 1×10^{-5} mol/L, respectively, while in the range of 5.43–18.96 nm, 4.65–7.66 nm, and 5.07–10.44 nm at 1×10^{-3} mol/L, respectively. It is suggested that the major monolayer formed accompanied by bilayer and multilayer structures at HMC. As the concentration increased to CMC, large columned micelles formed with bilayer and multilayer structures, along with further increase surface coverage (Figure 12c–h, Figure 13c–h). The concomitant monolayer, bilayer, and multilayer structure of unsaturated fatty acid molecules on the same surface were observed, which shows that before the completion of monolayer coverage on rhodochrosite surface, patches of bilayer structures formed, and the hydrophobic association of the hydrocarbon chains takes place. This effect may be attributed to the heterogeneity of mineral surface [61] and the self-assembly of unsaturated fatty acids in aqueous solution [20]. In contrast, the bilayer structure of SA did not appear before the monolayer coating, which may be due to the low compressibility of SA molecules resulting from the attraction between hydrocarbon chains of adjacent SA molecules. Therefore, a tight monolayer can be obtained in the adsorption process [34]. However, unsaturated fatty acids have large molecular spacing (Table 1) and weak intermolecular attraction due to the spatial hindrance caused by C=C double bond in their carbon chains. This will cause the monolayer structure to be loose during the adsorption process, resulting in the interspace on the surface easily overlaid by double-layer structures.

4. Conclusions

The θ of rhodochrosite increases with the increase in fatty acid concentration, reaching a maximum between HMC and CMC. Fatty acids containing C=C double bond have a higher maximum θ than SA, but the maximum decreases with an increase in the number of C=C double bonds. As the SA concentration increases, a monolayer with oriented structure can be formed on rhodochrosite surface with enhanced hydrophobicity, while the formation of bilayer structure appears at a concentration around its CMC. The steric hindrance caused by the introduction of C=C double bond leads to the preferential adsorption of OA, LA, and ALA on the liquid-air interface. The θ remains almost constant with the increasing concentration until HMC, mainly contributed to the lower value of Γ_{SL} than Γ_{LG}. Electrostatic interaction is the main driving force for the significant enhancement of rhodochrosite hydrophobicity. AFM researches suggest that small cylindrical monolayer and large cylindrical bilayer micelles formed on rhodochrosite surface as SA concentration arriving at its HMC and CMC, respectively. The concomitant monolayer and bilayer micelles adsorbed on rhodochrosite at HMC for OA, LA, and ALA, while the coexisting bilayer and multilayer structures on rhodochrosite at CMC due to the surface heterogeneity. Therefore, there is an appropriate concentration of fatty acid between HMC and CMC for rhodochrosite flotation.

Author Contributions: Conceptualization, Z.S. and Q.Z.; methodology, Z.S.; software, Z.S.; validation, Z.S., Q.Z. and Q.C.; formal analysis, X.L.; investigation, Z.S.; resources, Q.Z.; data curation, Z.S.; writing-original draft preparation, Z.S.; writing-review and editing, Z.S., Q.Z. and X.L.; visualization, Z.S.; supervision, Q.Z.; project administration, Q.C.; funding acquisition, Q.Z. All authors have read and agreed to the published version of the manuscript.

References

1. Chau, T.T.; Bruckard, W.J.; Koh, P.T.L.; Nguyen, A.V. A review of factors that affect contact angle and implications for flotation practice. *Adv. Colloid Interface Sci.* **2009**, *150*, 106–115. [CrossRef] [PubMed]
2. Aveyard, R.; Binks, B.P.; Clint, J.H. Emulsions stabilised solely by colloidal particles. *Adv. Colloid Interface Sci.* **2003**, *100*, 503–546. [CrossRef]
3. Ghosh Chaudhuri, R.; Paria, S. Effect of electrolytes on wettability of glass surface using anionic and cationic surfactant solutions. *J. Colloid Interface Sci.* **2014**, *413*, 24–30. [CrossRef] [PubMed]
4. Wang, C.; Cao, X.; Guo, L.; Xu, Z.; Zhang, L.; Gong, Q.; Zhang, L.; Zhao, S. Effect of adsorption of catanionic surfactant mixtures on wettability of quartz surface. *Colloids Surf. A Physicochem. Eng. Asp.* **2016**, *509*, 564–573. [CrossRef]
5. Wills, B.A.; Finch, J.A. *Wills' Mineral Processing Technology: An Introduction to the Practical Aspects of Ore Treatment and Mineral Recovery*, 8th ed.; Butterworth-Heinemann Elsevier Ltd.: Oxford, UK, 2016.
6. Wang, G.; Nguyen, A.V.; Mitra, S.; Joshi, J.B.; Jameson, G.J.; Evans, G.M. A review of the mechanisms and models of bubble-particle detachment in froth flotation. *Sep. Purif. Technol.* **2016**, *170*, 155–172. [CrossRef]
7. Han, C.; Li, T.; Zhang, W.; Zhang, H.; Zhao, S.; Ao, Y.; Wei, D.; Shen, Y. Density Functional Theory Study on the Surface Properties and Floatability of Hemimorphite and Smithsonite. *Minerals* **2018**, *8*, 542. [CrossRef]
8. Tripathy, S.K.; Mallick, M.K.; Singh, V.; Murthy, Y.R. Preliminary studies on teeter bed separator for separation of manganese fines. *Powder Technol.* **2013**, *239*, 284–289. [CrossRef]
9. Altun, N.E.; Hicyilmaz, C.; Hwang, J.Y.; Bagci, A.S. Evaluation of a Turkish low quality oil shale by flotation as a clean energy source: Material characterization and determination of flotation behavior. *Fuel Process. Technol.* **2006**, *87*, 783–791. [CrossRef]
10. Rao, S.R. *Surface Chemistry of Froth*; Springer: Berlin/Heidelberg, Germany, 2004.
11. Fuerstenau, M.C.; Jameson, G.J.; Yoon, R.H. *Froth Flotation: A Century of Innovation*; Society for Mining, Metallurgy, and Exploration, Inc.: Englewood, CO, USA, 2007.
12. Cao, X.; Lu, J.A.; Zhang, G. Flotation processing research of a low-grade manganese carbonate ore. *Metal Mine* **2013**, *42*, 99–101.
13. Fuerstenau, D.W.; Shibata, J. On using electrokinetics to interpret the flotation and interfacial behavior of manganese dioxide. *Int. J. Miner. Process.* **1999**, *57*, 205–217. [CrossRef]
14. Andrade, E.M.; Costa, B.L.C.M.; Alcantara, G.A.G.; Lima, R.M.F. Flotation of manganese minerals and quartz by sodium oleate and water glass. *Lat. Am. Appl. Res.* **2012**, *42*, 39–43.
15. Teng, Q.; Feng, Y.L.; Li, H.R.; Yang, Z.C. Dodecylamine flotation separation of rhodochrosite from calcite and its mechanism. *Chin. J. Nonferr. Metals* **2014**, *24*, 2676–2683. [CrossRef]
16. Zhang, Y.; Zhong, H.; Tan, X.; Zhan, J. Research progress in cationic collectors. *Conserv. Util. Miner. Resour.* **2011**, 44–49. [CrossRef]
17. Song, S.; Lopez-Valdivieso, A.; Ding, Y. Effects of nonpolar oil on hydrophobic flocculation of hematite and rhodochrosite fines. *Powder Technol.* **1999**, *101*, 73–80. [CrossRef]
18. Sis, H.; Chander, S. Reagents used in the flotation of phosphate ores: A critical review. *Miner. Eng.* **2003**, *16*, 577–585. [CrossRef]
19. Brandão, P.R.G.; Poling, G.W. Anionic flotation of magnesite. *Can. Metall. Quart.* **1982**, *21*, 211–220. [CrossRef]
20. Ye, J.; Zhang, Q.; Li, X.; Wang, X.; Ke, B.; Li, X.; Shen, Z. Effect of the morphology of adsorbed oleate on the wettability of a collophane surface. *Appl. Surf. Sci.* **2018**, *444*, 87–96. [CrossRef]
21. Xie, J.; Li, X.; Mao, S.; Li, L.; Ke, B.; Zhang, Q. Effects of structure of fatty acid collectors on the adsorption of fluorapatite (0 0 1) surface: A first-principles calculations. *Appl. Surf. Sci.* **2018**, *444*, 699–709. [CrossRef]
22. Lu, Y.; Drelich, J.; Miller, J.D. Oleate adsorption at an apatite surface studied by ex-situ FTIR internal reflection spectroscopy. *J. Colloid Interface Sci.* **1998**, *202*, 462–476. [CrossRef]
23. Young, C.A.; Miller, J.D. Effect of temperature on oleate adsorption at a calcite surface: An FT-NIR/IRS study and review. *Int. J. Miner. Process.* **2000**, *58*, 331–350. [CrossRef]
24. Rao, K.H.; Forssberg, K.S.E. Mechanism of fatty acid adsorption in salt-type mineral flotation. *Miner. Eng.* **1991**, *4*, 879–890. [CrossRef]
25. Iwasaki, I.; Cooke, S.R.B.; Choi, H.S. Flotation characteristics of hematite, goethite and acitivated quartz with 18-carbon aliphatic acids and related compounds. *Trans. AIME* **1960**, *217*, 237–244.

26. Purcell, G.; Sun, S.C. Significance of double bonds in fatty acid flotation-an electrokinetic study—A flotation study. *Trans. AIME* **1963**, *226*, 13–16.

27. Liu, R.; Zhang, G.; Zhang, H.; Liu, L.; He, L.; Chen, Y. Effect of iodine value of sodium fatty acids on flotation of collophanite. *Physicochem. Probl. Miner. Process.* **2019**, *55*, 770–778. [CrossRef]

28. Wang, Y.; Feng, Y.; Zhang, Q.; Lu, D.; Hu, Y. Flotation separation of diaspore from aluminosilicates using commercial oleic acids of different iodine values. *Int. J. Miner. Process.* **2017**, *168*, 95–101. [CrossRef]

29. Zhou, F.; Yan, C.; Wang, H.; Sun, Q.; Wang, Q.; Alshameri, A. Flotation behavior of four C18 hydroxamic acids as collectors of rhodochrosite. *Miner. Eng.* **2015**, *78*, 15–20. [CrossRef]

30. Zhou, F.; Chen, T.; Yan, C.; Liang, H.; Chen, T.; Li, D.; Wang, Q. The flotation of low-grade manganese ore using a novel linoleate hydroxamic acid. *Colloids Surf. A Physicochem. Eng. Asp.* **2015**, *466*, 1–9. [CrossRef]

31. Chen, J.Q.; Zhou, J.; Zou, Y.K.; Wan, Y.Y.; Chen, H.; Zhou, C.H.; Chen, T.; Yan, C.J. Flotation behavior and mechanism of low-grade manganese ore using N-hydroxyethyl fatty acid amide. *Chin J. Nonferr. Metals* **2018**, *28*, 1059–1066. (In Chinese) [CrossRef]

32. Dai, T.; Wang, S.; Zhong, H. Flotation performance and adsorption mechanism of alkyl-amide-hydroxime acid to rhodochrosite. *China' Manganese Ind.* **2018**, *36*, 142–146. (In Chinese) [CrossRef]

33. Qin, W.; Zou, S.; Liu, S.; Luo, H.; Liu, R.; Wang, X. Solution chemistry mechanism of flotation of sodium oleate on rhodochrosite. *J. Wuhan Univ. Technol.* **2014**, *36*, 124–129. [CrossRef]

34. Bu, Y.; Liu, R.; Sun, W.; Hu, Y. Synergistic mechanism between SDBS and oleic acid in anionic flotation of rhodochrosite. *Int. J. Miner. Metall. Mater.* **2015**, *22*, 447–452. [CrossRef]

35. Zhao, G.; Dai, T.; Wang, S.; Zhong, H. Study on a novel hydroxamic acid as the collector of rhodochrosite. *Physicochem. Probl. Miner. Process.* **2018**, *54*, 428–439. [CrossRef]

36. Tomoaia-Cotişel, M.; Zsako, J.N.; Mocanu, A.; Lupea, M.; Chifu, E. Insoluble mixed monolayers: III. The ionization characteristics of some fatty acids at the air/water interface. *J. Colloid Interface Sci.* **1987**, *117*, 464–476. [CrossRef]

37. Hifeda, Y.M.; Rayfield, G.W. Phase transitions in fatty acid monolayers containing a single double bond in the fatty acid tail. *J. Colloid Interface Sci.* **1985**, *104*, 209–215. [CrossRef]

38. Kanicky, J.R.; Shah, D.O. Effect of degree, type, and position of unsaturation on the pKa of long-chain fatty acids. *J. Colloid Interface Sci.* **2002**, *256*, 201–207. [CrossRef]

39. Davies, J.T.; Rideal, E.K. *Interfacial Phenomena*; Academic Press: New York, NY, USA, 1961.

40. Peltonen, J.P.K.; Rosenholm, J.B. Thin Solid Films. The influence of light on the properties of fatty acid-poly(3-octylthiophene) Langmuir-Blodgett films. *Thin Solid Films* **1989**, *179*, 543–547. [CrossRef]

41. Wang, X.; Zhang, Q. Insight into the Influence of Surface Roughness on the Wettability of Apatite and Dolomite. *Minerals* **2020**, *10*, 114. [CrossRef]

42. Xie, J.; Zhang, Q.; Mao, S.; Li, X.; Shen, Z.; Li, L. Anisotropic crystal plane nature and wettability of fluorapatite. *Appl. Surf. Sci.* **2019**, *493*, 294–307. [CrossRef]

43. Jin, G. *Surfactant Chemistry*, 2nd ed.; University of Science and Technology of China Press: Hefei, China, 2013.

44. Jiang, Y.C.; Ye, J.P.; Wu, S.K. Premicelle formation in surfactant solution and measurement of its average aggregation number. *Acta Chim. Sin.* **1992**, *50*, 1080–1084. (In Chinese)

45. Cao, Q.; Cheng, J.; Wen, S.; Li, C.; Bai, S.; Liu, D. A mixed collector system for phosphate flotation. *Miner. Eng.* **2015**, *78*, 114–121. [CrossRef]

46. Wang, Y.; Jiang, L.; Shen, Q.; Shen, J.; Hana, Y.; Hongman, Z. Investigation on the self-assembled behaviors of C18 unsaturated fatty acids in arginine aqueous solution. *RSC Adv.* **2017**, *7*, 41561–41572. [CrossRef]

47. Lundgren, S.M.; Persson, K.; Mueller, G.; Kronberg, B.; Clarke, J.; Chtaib, M.; Claesson, P.M. Unsaturated fatty acids in alkane solution: Adsorption to steel surfaces. *Langmuir* **2007**, *23*, 10598–10602. [CrossRef] [PubMed]

48. Wood, M.H.; Casford, M.T.; Steitz, R.; Zarbakhsh, A.; Welbourn, R.J.L.; Clarke, S.M. Comparative adsorption of saturated and unsaturated fatty acids at the iron oxide/oil interface. *Langmuir* **2016**, *32*, 534–540. [CrossRef] [PubMed]

49. Bernett, M.K.; Zisman, W.A. Relation of wettability by aqueous solutions to the surface constitution of low-energy solids. *J. Phys. Chem.* **1959**, *63*, 1241–1246. [CrossRef]

50. Bernett, M.K.; Zisman, W.A. Wetting of low-energy solids by aqueous solutions of highly fluorinated acids and salts. *J. Phys. Chem.* **1959**, *63*, 1911–1916. [CrossRef]

51. Szymczyk, K.; Zdziennicka, A.; Jańczuk, B.; Wójcik, W. The wettability of polytetrafluoroethylene and polymethyl methacrylate by aqueous solution of two cationic surfactants mixture. *J. Colloid Interface Sci.* **2006**, *293*, 172–180. [CrossRef]

52. Zdziennicka, A.; Janczuk, B.; Wójcik, W. Wettability of polytetrafluoroethylene by aqueous solutions of two anionic surfactant mixtures. *J. Colloid Interface Sci.* **2003**, *268*, 200–207. [CrossRef]

53. Bargeman, D.; Van Voorst Vader, F. Effect of surfactants on contact angles at nonpolar solids. *J. Colloid Interface Sci.* **1973**, *42*, 467–472. [CrossRef]

54. Lucassen-Reynders, E.H. Surface equation of state for ionized surfactants. *J. Phys. Chem.* **1966**, *70*, 1777–1785. [CrossRef]

55. Zhang, L.; Wang, Z.; Li, Z.; Zhang, L.; Xu, Z.; Zhao, S.; Yu, J. Wettability of a quartz surface in the presence of four cationic surfactants. *Langmuir* **2010**, *26*, 18834–18840. [CrossRef]

56. Li, Z.; Zhang, L.; Xu, Z.; Liu, D.; Song, X.; Cao, X.; Zhang, L.; Zhao, S. Effect of zwitterionic surfactants on wetting of quartz surfaces. *Colloids Surf. A Physicochem. Eng. Asp.* **2013**, *430*, 110–116. [CrossRef]

57. Zisman, W.A. Contact angle, wettability and adhesion. In *Advances in Chemistry Series*; Gould, R.F., Ed.; American Chemical Society: Washington, DC, USA, 1964.

58. McMurry, J.E. *Organic Chemistry*, 6th ed.; Brooks Cole: Monterey, CA, USA, 2003.

59. Al-Busaidi, I.K.; Al-Maamari, R.S.; Karimi, M.; Naser, J. Effect of different polar organic compounds on wettability of calcite surfaces. *J. Petrol. Sci. Eng.* **2019**, *180*, 569–583. [CrossRef]

60. Xie, Z.; Jiang, H.; Sun, Z.; Yang, Q. Direct AFM measurements of morphology and interaction force at solid-liquid interfaces between DTAC/CTAC and mica. *J. Cent. South Univ.* **2016**, *23*, 2182–2190. [CrossRef]

61. Chennakesavulu, K.; Raju, G.B.; Prabhakar, S.; Nair, C.M.; Murthy, K.V.G.K. Adsorption of oleate on fluorite surface as revealed by atomic force microscopy. *Int. J. Miner. Process.* **2009**, *90*, 101–104. [CrossRef]